Supporting Information

Revealing the Charge Density Wave Proximity Effect in Graphene on 1T-TaS_2

Michael A. Altvater[1], Sheng-Hsiung Hung[2], Nikhil Tilak[1], Guohong Li[1], Choong-Jae Won[3], Sang-Wook Cheong[1], Chung-Hou Chung[4], Horng-Tay Jeng[2] and Eva Y. Andrei[1]*

Removing Graphene with STM Tip

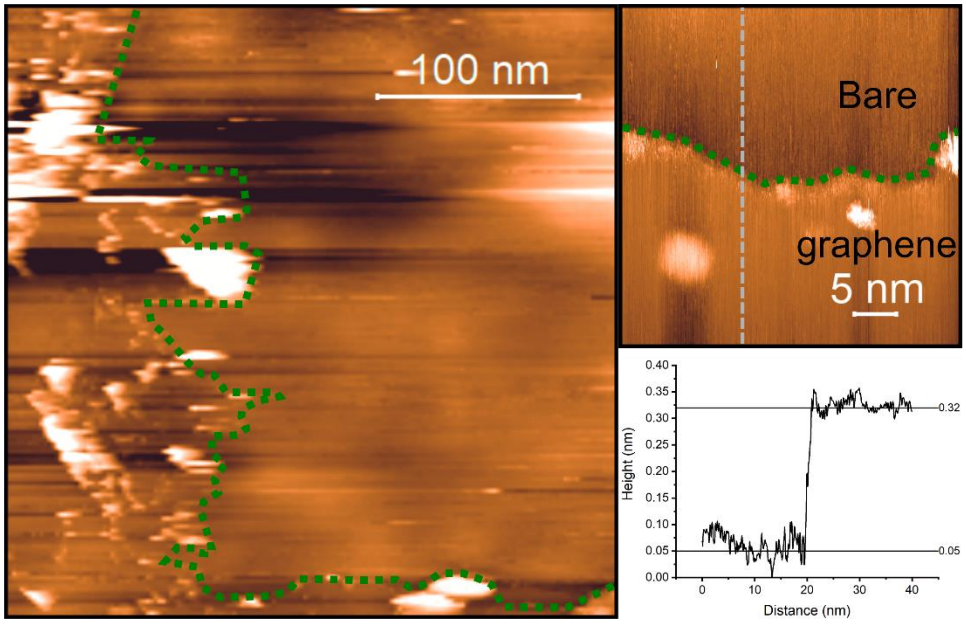

Figure S1: a) Large area topography image at the corner where graphene has been removed from the TaS_2 surface. Edge of graphene is outlined with a green, dashed line. b) Zoomed in image of the graphene edge, highlighted with a green, dashed line. c) Linecut along the gray dashed line in (b) showing a step across the graphene edge showing a 0.27±0.07 nm step

We find that for low biases and large set currents (when the tip is near the surface), the graphene layer is able to be lifted by the STM tip. This tip-graphene interaction allows us to peel a region of graphene off of the 1T-TaS_2 surface at 77K, exposing a region of bare 1T-TaS_2.

Moiré Pattern Between Graphene and TaS_2

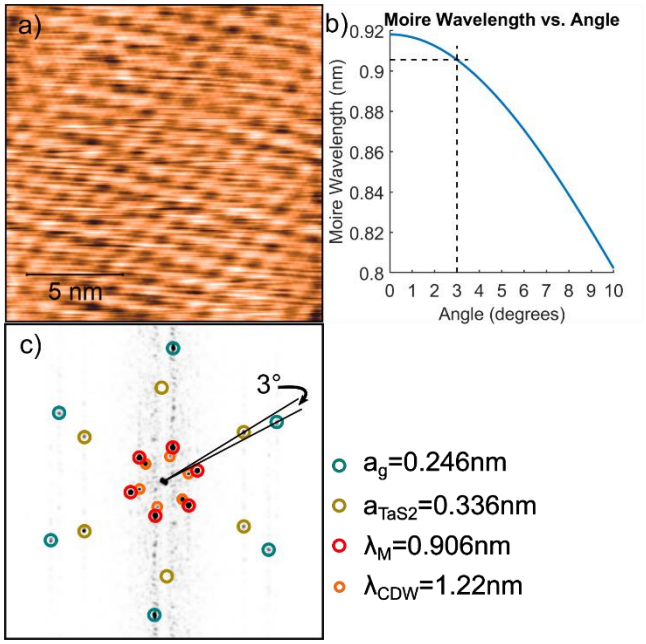

Figure S2: a) STM topography displaying a Moiré interference pattern as well as charge density wave modulation (V_b=0.550V, I_{SP}=150pA) b) Plot of the expected Moiré pattern wavelength between the graphene and TaS_2 lattices as a function of angle. The experimentally determined value is marked with dashed lines c) Fourier transform of the topography image in (a) shows peaks associated with the graphene lattice ($a_g = 0.246nm$ is assumed), 1T-TaS_2 lattice (measured $a_{TaS2} = 0.336nm$), the induced Moiré wavelength (measured $\lambda_M = 0.906nm$), and the commensurate CDW (measured $\lambda_{CDW} = 1.22nm$)

In a different region of the structure and at a different bias voltage than shown in the main text, we more clearly resolve the graphene and TaS_2 lattices [Figure S2(a)]. The structure observed is different than that of the previous region [figure 1, main text]. The differences can be identified more clearly by viewing the FFT of the real space image [Figure S2(c)]. In the Fourier transform we can find 4 sets of Bragg peaks with different wavevectors. For accuracy, we compare the measured wavevectors to that of the graphene lattice [the outermost set of peaks in figure S2(c)]. We find that the other 3 sets of peaks correspond to the periodic modulations of the TaS_2 lattice ($a_{TaS2} = 0.336nm$), the commensurate charge density wave ($\lambda_{CDW} = 1.22nm$), as well as a modulation with period $\lambda = 0.906nm$. It is known that interference between two misaligned periodic patterns leads to a Moiré superpattern, observable by STM. The well-known relationship between the Moiré period and the crystal lattice mismatch is given by:

$$\lambda_M = \frac{(1+\delta)a_g}{\sqrt{2(1+\delta)(1-\cos\theta)+\delta^2}}$$

For the lattice mismatch between the graphene and TaS_2 lattice, $\delta = \frac{a_{TaS2}}{a_g} - 1 \approx 0.366$, the Moiré wavelength as a function of angle is plotted at low angles in Figure 5(b). We can use the positions of the Bragg peaks associated with crystalline lattices to determine the angle between graphene and TaS_2 in this region to be approximately $\theta = 3°$. Thus, we identify the unknown periodic modulation as the Moiré pattern induced by interference between the graphene and TaS_2 lattices.

Kohn Anomalies and CDW Supercell

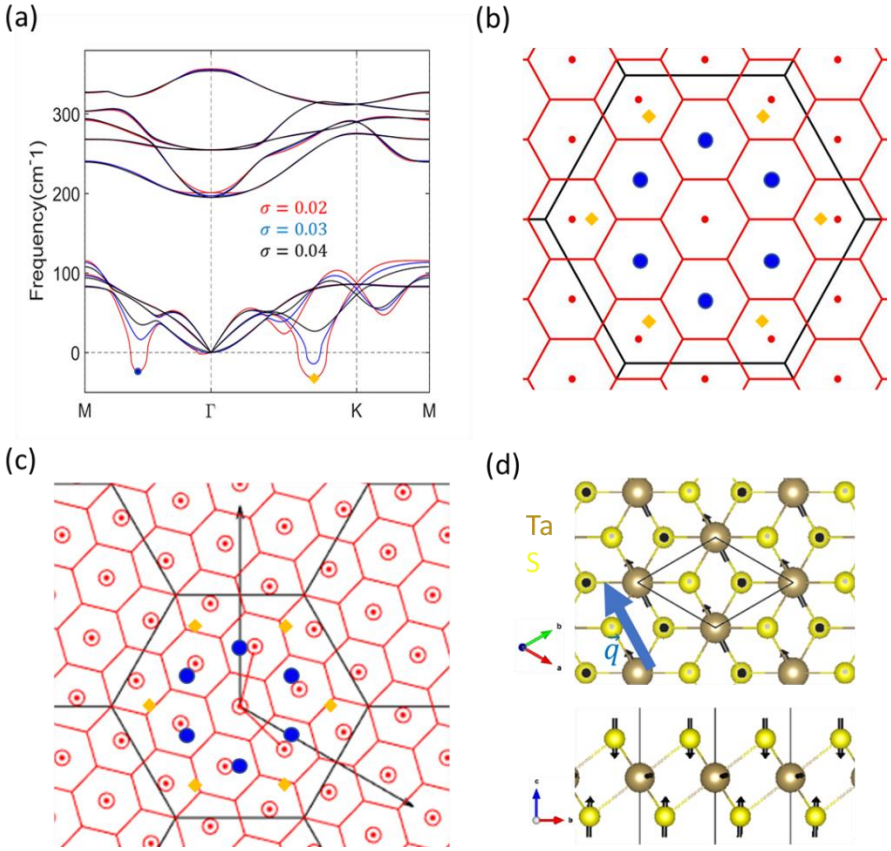

Figure S3: a) Phonon dispersion of undistorted 1T-TaS_2. The Kohn anomaly wavevectors are marked by blue circle and yellow rhombus. Different broadening values σ indicate the temperature effect. b) Kohn anomaly wavevectors and Brillouin zone (BZ) of 1×1 (black) and $\sqrt{13} \times \sqrt{13}$ (red) structures. The blue Kohn anomaly wavevector **q** along ΓM locates at the zone centers of the $\sqrt{13} \times \sqrt{13}$ CDW BZs, whereas the yellow Kohn anomaly wavevector along ΓK does not fit the $\sqrt{13} \times \sqrt{13}$ CDW BZs. (c) The $\sqrt{13} \times \sqrt{13}$ CDW BZs are rotated to form the commensurate BZs. d) Ta atoms vibrate parallel to the Kohn anomaly wavevector **q**, while S atoms vibrate perpendicularly to **q**.

The calculated phonon dispersion for the unreconstructed 1T-TaS_2 in Fig. S3(a) shows two Kohn anomalies, phonon modes whose frequencies drop to (or below) zero, indicating a lattice instability. These Kohn anomalies can be stabilized without negative frequency by using higher broadening (σ) values. This corresponds to the removed CDW phase at higher temperatures observed in experiments.

The blue Kohn anomaly instability at wavevector **q** coincides with the wavevector $\mathbf{Q_{CDW}}$ of the $\sqrt{13} \times \sqrt{13}$ CDW reconstruction, suggesting electron-phonon coupling as a possible origin for the CDW. Fig. S3(b) demonstrates that the blue Kohn anomaly wavevector **q** along ΓM locates at the zone centers of the $\sqrt{13} \times \sqrt{13}$ CDW BZs. The good match in the periodicity indicates the tendency from 1x1 unit cell toward the $\sqrt{13} \times \sqrt{13}$ CDW lattice. Although the q vector of 1x1 unit cell matches the period of $\sqrt{13} \times \sqrt{13}$ BZ, it is not possible for the 1x1 BZ to match the non-integer $\sqrt{13} \times \sqrt{13}$ BZ. This actually suggests a ~13.9° rotation of the $\sqrt{13} \times \sqrt{13}$ BZ as shown in Fig. S3(c). The rotated $\sqrt{13} \times \sqrt{13}$ supercell thus commensurate with the 1x1 unit cell as observed and discussed in this work experimentally and theoretically. On the other hand, the yellow Kohn anomaly does not fit the BZ of possible minimum supercells and thus is not observed. The blue soft phonon mode at the Kohn anomaly wavevector **q** contains mainly longitudinal vibration of Ta atoms with minor transverse vibration of S atoms relative to the phonon propagating direction **q** as depicted in Fig. S3(d).

CDW Induced Isolated Flat Band

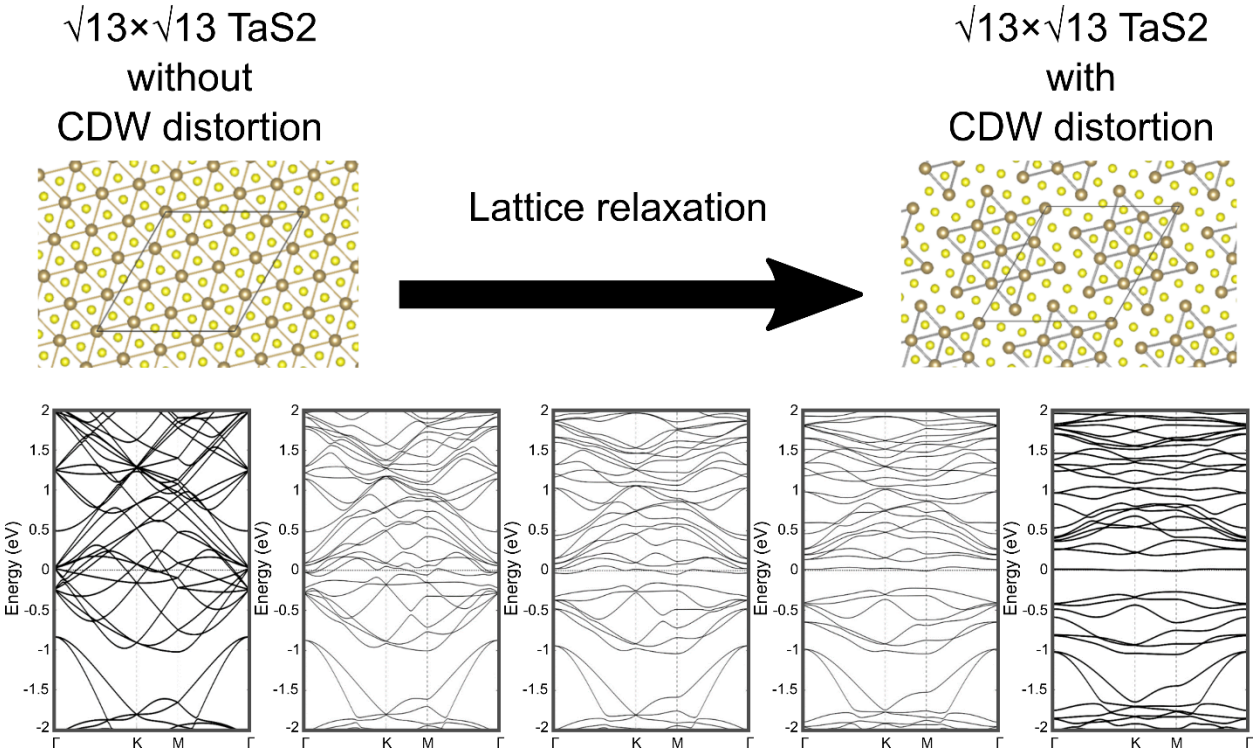

Figure S4: Evolution of the GGA band structure (bottom) as the lattice relaxes (from left to right) from the undistorted lattice structure (shown top, left) to the $\sqrt{13} \times \sqrt{13}$ distortion (top, right)

The undistorted 13 Ta atoms within the $\sqrt{13} \times \sqrt{13}$ supercell (top-left panel), the same size as the CDW unit cell (top-right panel), each contribute one conduction electron to the undistorted band structure (bottom-left panel). As the lattice is allowed to relax, 6 of these Ta-associated bands are pushed below the Fermi level while 6 are pushed to higher energies, leaving a single, flat, isolated band at the Fermi level (bottom-right panel). This band is associated with an electron state localized at the

center of the Stars of David in the CDW reconstructed structure (top-right panel). As a flat, isolated band, the electronic kinetic energy (and kinetic energy spread) is low, allowing interparticle interactions to dominate and correlated electronic phases can emerge.

Hubbard U Enhanced Gap

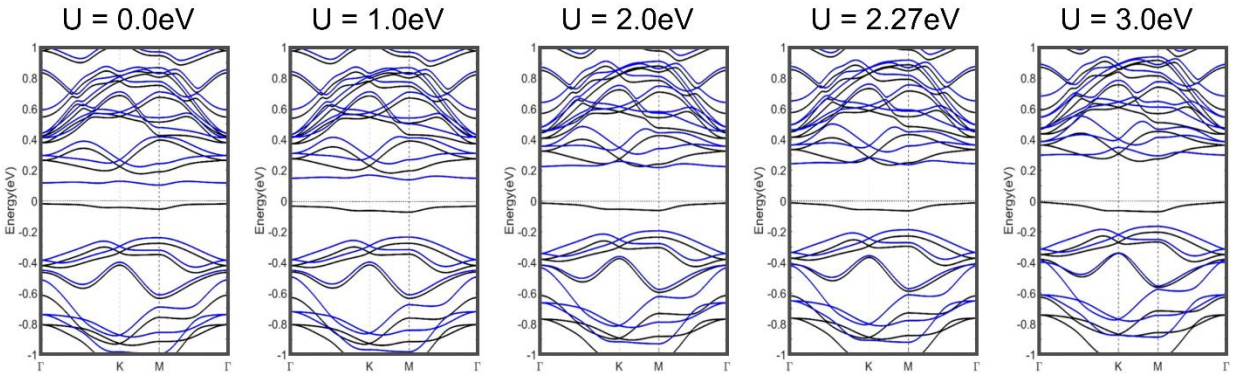

Figure S5: Evolution of the GGA+U band structure with increasing values of Hubbard U from 0 to 3 eV.

In the 1T-TaS_2 monolayer, the DFT calculation shows an exchange gap at the Fermi level, even without including a Hubbard U. However, this gap is much smaller than that measured experimentally. To reproduce experimental observations, a Hubbard U is added to the calculation to encompass Coulomb repulsion between electrons in neighboring CDW stars. Increasing the value of U enhances the gap at the Fermi level. The value of U=2.27eV, previously determined from linear response theory, is used in the calculations given in the main text.

CDW, Exchange, and Mott gaps

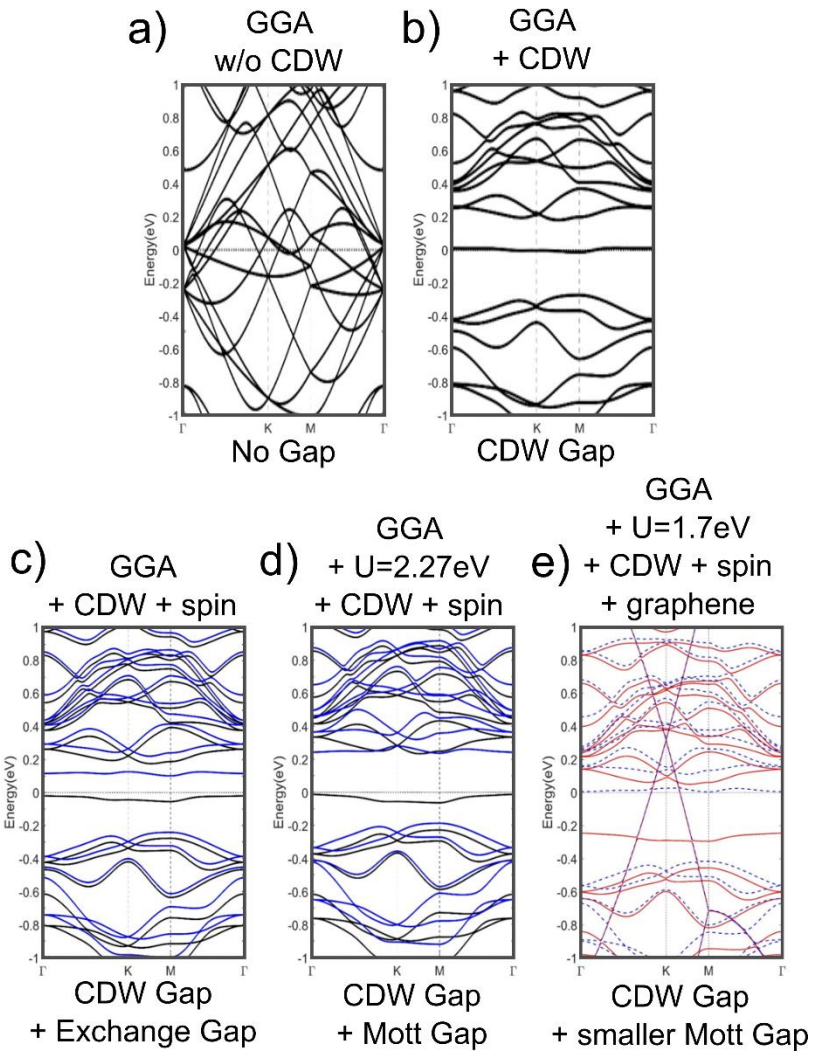

Figure S6: a) GGA band structure of undistorted 1T-TaS_2 shows no band gap. b) After relaxing the lattice, a CDW gap opens with an in-gap, half-filled, isolated flat band stuck at E_F. c) Adding spin splits the isolated flat band into two spin-polarized bands separated by an exchange gap. d) Increasing the on-site Hubbard U expands the exchange gap into the experimentally observed Mott gap. e) With the addition of graphene, the Hubbard U and the associated Mott gap are reduced in size due to screening from the graphene layer.

The outline of the emergence of the insulating state of 1T-TaS_2 begins with the CDW lattice reconstruction which isolates a narrow, flat band at the Fermi level within the CDW-induced gap. Including spin freedom and exchange interactions, the flat band splits into an exchange gap at the Fermi level. Adding a Hubbard U, enhances the gap into a Mott gap which reproduces experimental observations. Finally, adding a graphene layer on top causes a shift of the 1T-TaS_2 bands toward lower energies and adds a Dirac cone, centered at the K-points of the superstructure Brillouin zone. Additionally, the graphene layer is found to reduce the spacing between the Upper and Lower Hubbard bands of 1T-TaS_2 which is captured by using a smaller value of Hubbard U=1.70eV.

Bilayer 1T-TaS_2

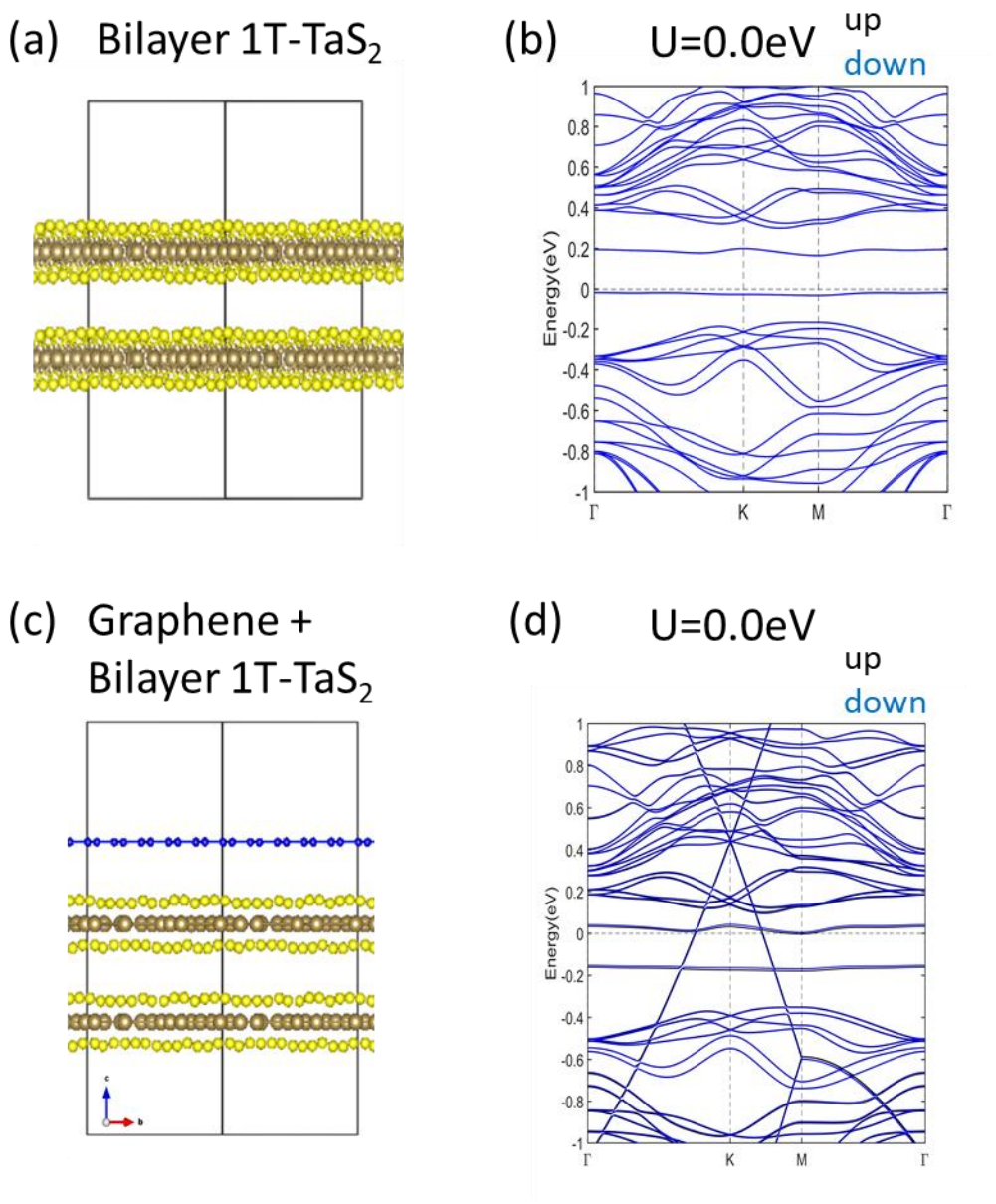

Figure S7: a) Ball and stick model of the unit cell used in the bilayer 1T-TaS_2 calculation with CDW clusters aligned along the c-axis. b) Calculated band structure of bilayer 1T-TaS_2 gives band insulating behavior as interlayer dimerization forms occupied and unoccupied bonding and anti-bonding states with no net magnetic moment. c) Ball and stick model of the unit cell used to calculate the band structure of graphene on bilayer 1T-TaS_2. 5x5 unit cells of graphene are placed on top of the bilayer 1T-TaS_2 structure used in (a). d) Band structure of the G/ bilayer 1T-TaS_2 heterostructure shows that the flat bands of the bilayer 1T-TaS_2 and the Dirac cone of graphene are preserved in the heterostructure as well as a ~7.7% reduction of the spacing between flat bands with the addition of graphene.

We firstly calculated the total energies for different stacking configurations of 1T-TaS2 bilayer with van der Waals interaction included. Our calculations conclude that the AA stacking is more stable in

dimerized bilayer 1T-TaS2. Another related calculation for bulk 1T-TaS2 can be found in [14]. Next, we use the AA stacking bilayer 1T-TaS_2 with Graphene on top as our lattice model and calculate the band structure. The flat band from each single layer 1T-TaS_2 is in the ferromagnetic state. The two ferromagnetic states of the bilayer rearrange their spins into the antiparallel singlet state as the two layers are dimerized. Hence, bilayer TaS2 has no total magnetic moment. Adding graphene to bilayer 1T-TaS_2 has similar effect as the monolayer 1T-TaS_2 case. First, charge transfer from Graphene to 1T-TaS_2 shifts the Dirac cone above fermi level [Fig. S7(d)]. The charge transfer corresponds to hole doping in graphene and shows charge modulations with the same pattern as the start-shape CDW of 1T-TaS_2. Second, the charge transfer also causes the reduction of the gap between two flat bands [Figs. S7(b,d)].